ELSEVIER

Thermochimica Acta 299 (1997) 19–25

thermochimica acta

Electrochemical intercalation of lithium into hexagonal tungsten trioxide

Naoaki Kumagai*, Aishui Yu, Nobuko Kumagai, Hitoshi Yashiro

Department of Applied Chemistry and Molecular Science, Faculty of Engineering, Iwate University, Morioka 020, Japan

Abstract

The kinetics and thermodynamics of electrochemical intercalation of lithium into hexagonal WO_3 prepared by a solution technique were studied with an a.c. impedance method, open-circuit potential and X-ray diffraction measurements. The open-circuit potential–x in Li_xWO_3 curve consists of two straight lines with different slopes, which was related to the structural variation in the oxide with lithium intercalation. The standard Gibbs energy of lithium intercalation, ΔG_l^0, was −239.4 kJ/mol in the range of x from 0 to 1 in Li_xWO_3 at 25°C. The chemical diffusion coefficient of lithium, $\tilde{D}$, for the intercalation into the oxide, was measured by a.c. impedance method as functions of depth of lithium intercalation and temperature in 1 M $LiClO_4$/propylene carbonate solution. The results showed that the Warburg impedance was linearly related to $\omega^{-1/2}$ (ω: angular frequency) and the ($\tilde{D}$) values obtained decreased with an increase in lithium concentration in the oxide, being one–two orders of magnitude higher than that in monoclinic WO_3. Furthermore, the lithium diffusion coefficient of lithium and the activation energy for the diffusion were also obtained as a function of x-value in Li_xWO_3.

Keywords: Electrochemical lithium intercalation reaction; Hexagonal tungsten trioxide; Kinetics; Thermodynamics

1. Introduction

Tungsten oxides have been extensively studied in recent years because of their electrochemical and electronic properties which make them attractive as active electrodes for secondary lithium batteries and electrochronomic display [1,2]. In order to improve the electrochemical performance of WO_3 as an electrode material, a great deal of work has been done upon the preparation, structure and electrochemical behavior [3,4]. The structure of the WO_3 host material plays an important role to the thermodynamics and kinetics of lithium intercalation into the oxide. The WO_6 octahedral building blocks join at the corners, which results in a variety of crystalline structures. In an effort to synthesize new compounds with interesting structure and ionic properties, a variety of preparation techniques [5–7] have been proposed. Gerand et al. [6] have prepared a hexagonal WO_3 by a complete dehydration of $WO_3 \cdot 1/3H_2O$, which was obtained by hydrothermal treatment of an aqueous suspension of tungstic acid at 120°C. Recently, we have prepared the hexagonal form of tungsten trioxide by a complete dehydration of $WO_3 \cdot yH_2O$($y = 0.8$–1.1), which was formed by acidification of aqueous lithium tungstate solution with a strong acid at ca. 100°C under ambient pressure [7]. Furthermore, we have examined the electrochemical lithium intercalation behavior as a cathode for secondary lithium batteries [7]. In the present paper, the kinetics and thermodynamics of electrochemical intercalation of lithium into the hexagonal WO_3 will be studied.

2. Experimental

Hexagonal tungsten is the product of total dehydration by the heat-treatment of a hydrate $WO_3 \cdot yH_2O$

*Corresponding author.

0040-6031/97/$17.00
PII S0040-6031(97)00131-7

($y = 0.8$–1.1). This hydrate was prepared by acidification of aqueous Li_2WO_4 solution with strong acid at a concentration of (0.5–1) M at ca. 100°C. Details on the preparation and identification of the hexagonal WO_3 were given in Ref. [7].

The cathode and cell preparation were described in Refs. [3,7]. The mixture of tungsten trioxide and graphite as a conducting agent, in a weight ratio of 1 : 1, was compressed on a nickel net under ca. 50 MPa and the pellet thus obtained was used as a working electrode after drying under vacuum at 25°C for one day. Typical cathode loading was ca. 10 mg/cm^2 (active material). The electrolyte used was 1 M propylene carbonate (PC)/$LiClO_4$ solution containing only trace amounts of water < 20 mg/dm^3 and lithium pellets were used for both the reference and the counter electrodes. Investigation was undertaken using a glass beaker type cell at room temperature in a dry box under argon atmosphere.

The open-circuit potentials (OCVs) were measured after 24 h equilibrium on open circuit at a constant temperature, when the potential was stabilized to < ±0.1 mV/h.

Details on the impedance measurements were also given in Ref. [3]. The frequency range used for the a.c. impedance was from (1 to 63) kHz, and the results were presented with a complex impedance plane. The cell used for the measurement was dipped in an oil bath and the temperature was controlled at < ±1.0°C. Before the a.c. measurement, the potential of the oxide electrode was in equilibrium for a few hours and the OCV was stabilized to less than < ±0.2 mV/h at a constant temperature.

Powder X-ray diffraction (XRD) measurement of the discharge products of the tungsten oxide was conducted using a Rigaku Denki Geiger flex 20B measurement with CuK_α radiation.

3. Results and discussion

3.1. Thermodynamics of lithium intercalation into hexagonal tungsten trioxide

The basic structural element of the hexagonal tungsten trioxide is an infinite plane of WO_6 octahedra sharing their corners and forming six-membered rings in the (001) plane [6]. The complete structure arises from stacking such layers perpendicular to the c-axis (Fig. 1). Our previous studies [7] have shown that the discharge process of hexagonal WO_3 as a positive electrode for lithium batteries includes lithium intercalation into the vacant channels without a significant change in the host matrix, so that the electrode reaction can be described as follows:

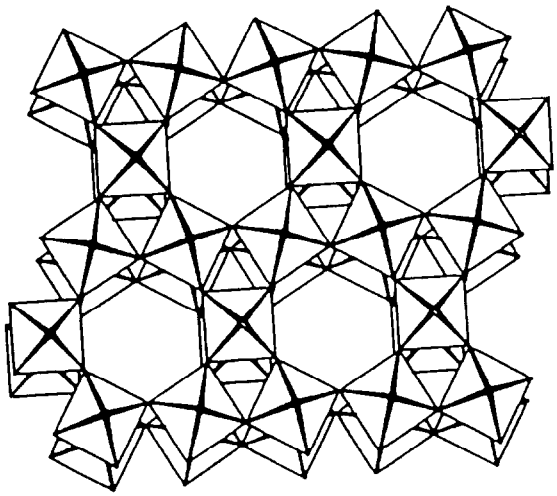

Fig. 1. Structure of hexagonal WO_3 with the hexagonal empty tunnels running along the [001] axis.

$$xLi^+ + xe^- + WO_3 = Li_xWO_3 \quad (1)$$

The variations in the OCVs of hexagonal WO_3 electrode at 25°C at a depth of lithium intercalation, x, are given in Fig. 2. The figure shows that the OCVs decrease linearly with an increase in the x-value in Li_xWO_3 and the OCV–x curve consists of two straight lines with different slopes at ca. $x \leq 0.8$ and $x > 0.8$. The relationships between the OCV (E) and the x-value are represented by

$$E = -2.97 - 0.91x \quad (x \leq 0.8) \quad (2)$$

$$E = 2.34 - 0.29x \quad (x > 0.8) \quad (3)$$

These results suggest that the intercalated lithium atoms occupy more than one kind of crystallographic sites and a single phase of Li_xWO_3, where the x-value varies continuously, is formed. The standard Gibbs energy of lithium intercalation, ΔG_I^0, in WO_3 was

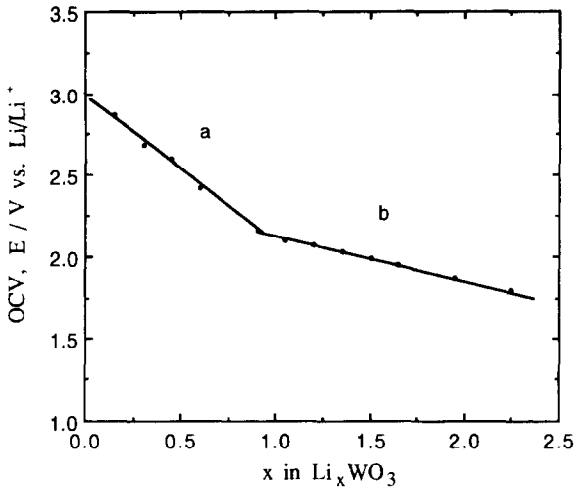

Fig. 2. Open-circuit potential as a function of depth of lithium intercalation, x, at 25°C.

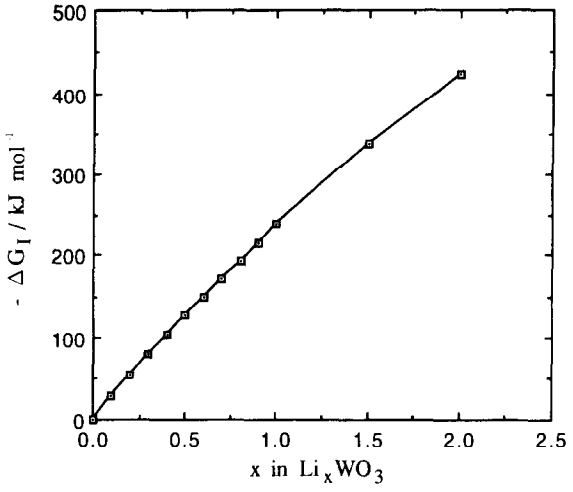

Fig. 3. Standard Gibbs energy of lithium intercalation as a function of x-values in Li_xWO_3.

calculated from the following equations:

$$\mu_{Li} - \mu^0_{Li} = RT \ln a_{Li} = -FE(x) \quad (4)$$

$$\Delta G^0_I = -F \int_o^x E(x)dx \quad (5)$$

where $E(x)$ is the open-circuit potential at respective x-value, and μ_{Li}, μ^0_{Li} and a_{Li} are the lithium chemical potential, the chemical potential for pure lithium and the activity of lithium, respectively [8]. The ΔG^0_I values obtained as a function of depth of lithium intercalation, x, are given in Fig. 3. As can be seen from the figure, the ΔG^0_I values increase with an increase in the x-value, being -239.4 kJ/mol at $x = 1$ and -423.2 kJ/mol at $x = 2$.

The variation in the crystal structure of hexagonal WO_3 with depth of lithium intercalation was examined by XRD method as shown in Fig. 4. As seen from the figure, the original crystal lattice was maintained during lithium intercalation up to $x = 2.0$. The discharge products could be indexed in an orthorhombic cell, and the crystallographic parameters of the discharge products for the oxide at different depths of lithium are given in Table 1. As can be seen in the table, the a- and b-lattice parameters increased slightly with lithium intercalation, whereas the c-lattice parameter and the unit cell volume decreased with lithium intercalation in the $0 < x < 0.5$ range of x-values, while they increased in the $0.5 < x < 2$ range. Such a structural variation probably corresponds to the OCV–x curve with two different slopes shown in Fig. 2. Furthermore, the ratios of b/a in the discharge products are close to $\sqrt{3}$. The X-ray results reveal that the unsolvated Li^+ ions are intercalated into the empty channels while maintaining the hexagonal-type structure.

3.2. *Kinetic characteristics of lithium into hexagonal WO_3*

Typical a.c. impedance responses of hexagonal Li_xWO_3 electrodes with different x-values measured at 30°C are shown in Fig. 5. The a.c. responses consist of an irregular semi-circular arc at high frequency and a spike at a low frequency. As can be seen in Fig. 5, all the centers of the circular arc observed at a high frequency are under zero horizon. This phenomena is probably due to the microscopic surface roughness of the porous electrode as discussed by de Levie [9]. However, at a low frequency, the double-layer capacitance becomes completely blocked, and the constant phase-angle Warburg impedance, Z_W, is clearly resolved. The low-frequency spikes are found with a phase angel of ca. 45°, thus the a.c. impedance responses can be simply modeled by Randles equivalent circuit [10] shown in Fig. 6, where R_0 is the uncompensated ohmic resistance of the electrode and electrolyte, C_{dl} is the double-layer capacitance

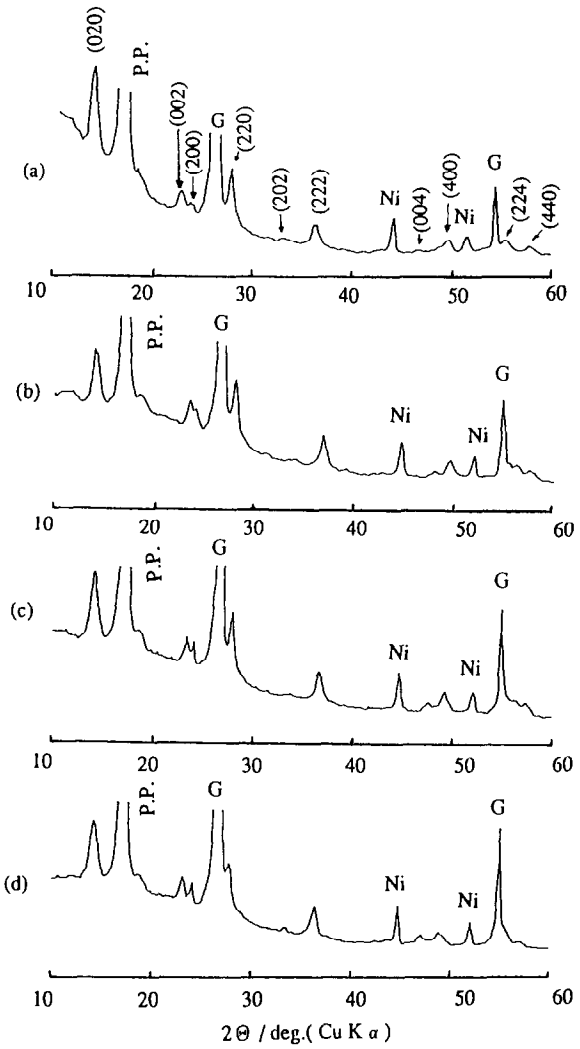

Fig. 4. X-ray diffraction patterns of Li_xWO_3 with various x-values: (a) – $x = 0$; (b) – $x = 0.5$; (c) – $x = 1.0$; (d)– $x = 2.0$. G – graphite; Ni – nickel net; P.P. – polypropylene film.

of the electrode–electrolyte interface, R_{ct} is the charge-transfer resistance. Ho et al. [11] obtained the following expression for Z_W by solving Fick's law with appropriate initial and boundary conditions:

$$Z_W = A_W \omega^{-1/2} \tag{6}$$

where ω is the angular frequency of the a.c. perturbation. The Warburg prefactor, A_W, is related to the chemical diffusion coefficient, $\tilde{D}$, of the electroactive species in electrode by

$$A_W = V_m(dE/dx)/zFA\tilde{D}^{1/2} \tag{7}$$

where V_m is the molar volume of the tungsten oxides (37.9 cm^3) [7], dE/dx the slope of the OCV/x-value in the Li_xWO_3 curve (Fig. 2), z the charge transfer number for lithium intercalation reaction (Eq. (1)), which is equal to one, A the electroactive surface area of the electrode, and a geometric area (1.4 cm^2) is used in the present study. Typical plots of observed Z_W against $\omega^{-1/2}$ are shown in Fig. 7 and the values of A_W obtained were found in the (1.49–2.33) $\Omega\ s^{-1}$ range of x-values in the (0.1–1.6) range.

As discussed by Weppner and Huggins [12], the chemical diffusion coefficient is related to the component diffusion coefficient for lithium, D_{Li}, by the following equation:

$$\tilde{D} = D_{Li}\,d(\ln a_{Li})/d(\ln C_{Li}) = D_{Li}(F/RT)(dE/dx) \tag{8}$$

where $d(\ln a_{Li})/d(\ln C_{Li})$ is the thermodynamic enhancement factor which is calculated from dE/dx, and R is the gas constant.

As seen in Eq. (7), the diffusion coefficient depends strongly on the effective surface area. Particularly in the porous oxide–graphite composite electrode of the

Table 1
Lattice parameters of Li_xWO_3 with various x-values

x in Li_xWO_3	Lattice parameter				Unit cell volume/ nm^3
	a/nm	b/nm	c/nm	b/a	
0	0.7293	1.263	0.7750	1.732	0.7167
0.5	0.7369	1.272	0.7572	1.728	0.7089
1.0	0.7406	1.269	0.7619	1.712	0.7160
2.0	0.7456	1.283	0.7707	1.721	0.7372

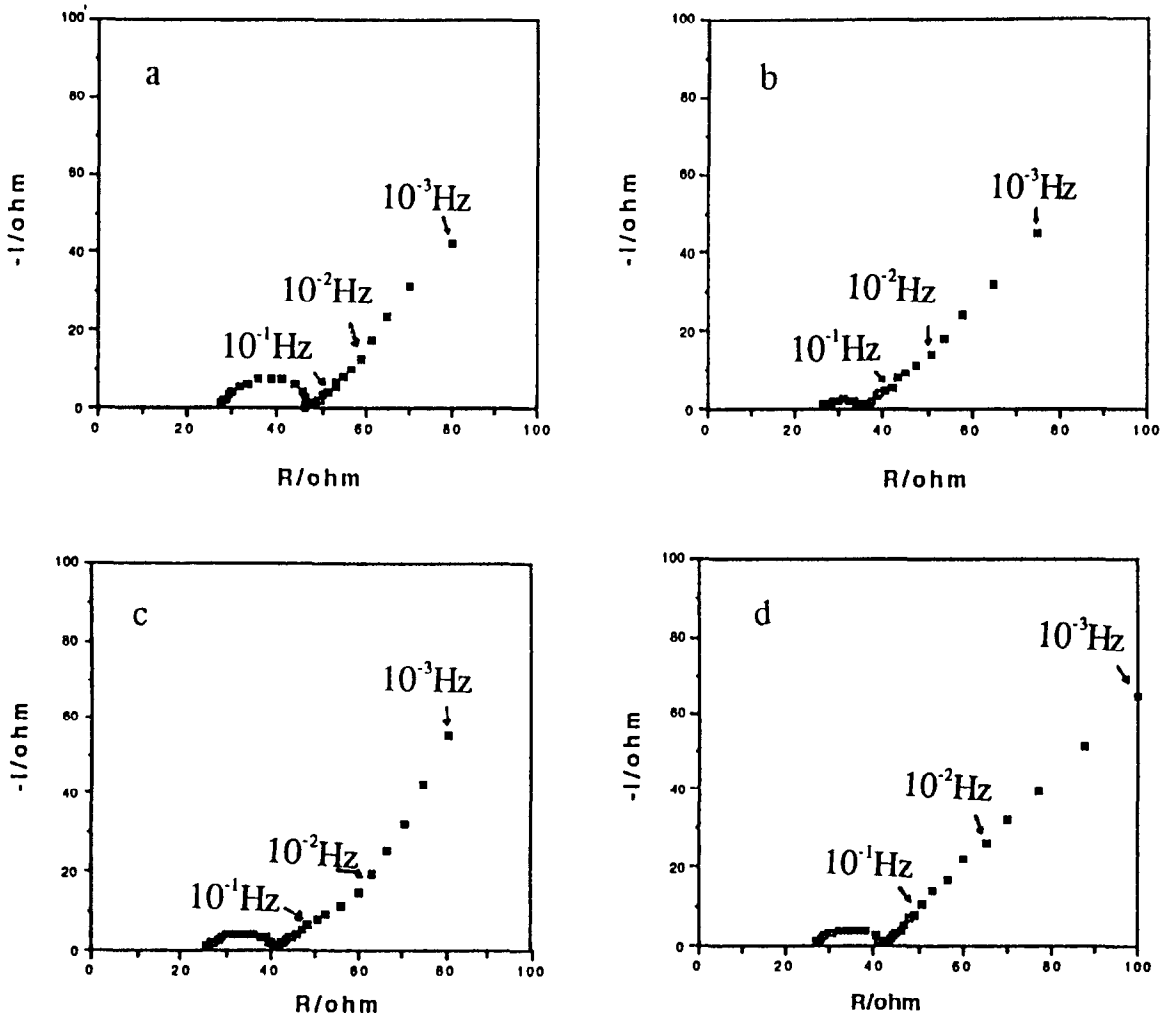

Fig. 5. Typical impedance diagrams for Li_xWO_3 electrodes in 1 M $LiClO_4$–PC solution: (a) – $x = 0.3$; (b) – $x = 0.5$; (c) – $x = 0.8$; and (d) – $x = 1.6$.

polycrystalline oxide, the geometric area used in the present work may be insufficient to calculate the diffusion coefficient. However, during the entire measurement, just one cell was used and the discharge process of the cell is unlikely to change the effective surface area of the electrode. Therefore, the values of $\tilde{D}$ probably reflect the actual variation in the lithium diffusion coefficients with different x-values in Li_xWO_3 and temperature. The calculated $\tilde{D}$ and D_{Li} values are shown in Fig. 8, as a function of depth of lithium intercalation. The $\tilde{D}$ and D_{Li} values for Li_xWO_3 electrode are of ca. 10^{-9} cm^2/s and ca. 10^{-10} cm^2/s, respectively, in the (0.3–1.6) range of x-values.

The lithium-component diffusion coefficient decreases with an increase in the x-value, which is consistent with the non-interacting lattice gas model [13], that is, a steady decrease in the diffusion coefficient with an increase in lithium concentration is predicted, due to decreasing probability of finding an unoccupied site next to an occupied one.

The complex plane diagrams of hexagonal Li_xWO_3 electrodes were measured in the (25–60)°C temperature range by the a.c. impedance method. The a.c.

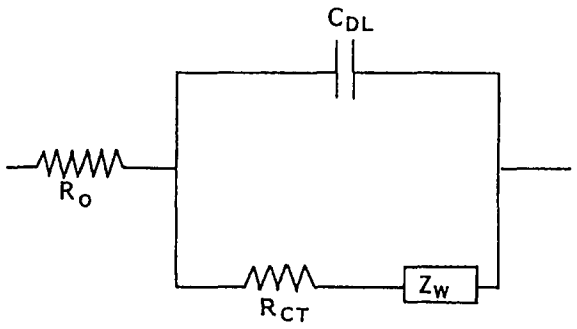

Fig. 6. The Randles equivalent circuit for a.c. responses.

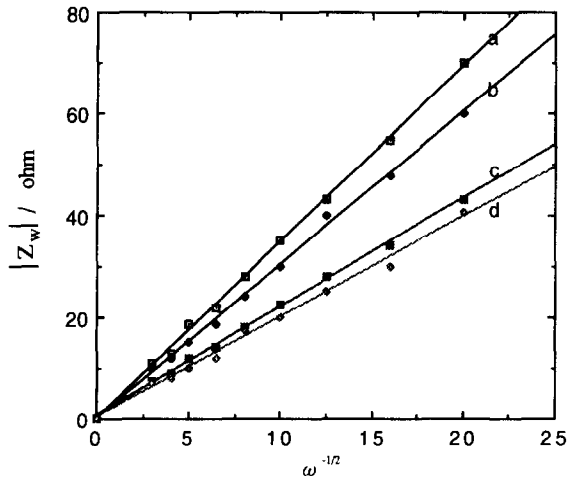

Fig. 7. Plots of observed Warburg impedance Z_W against $\omega^{-1/2}$ for Li_xWO_3 electrode at 30°C: (a) – $x = 0.1$; (b) – $x = 0.5$; (c) – $x = 0.8$; and (d) – $x = 1.6$.

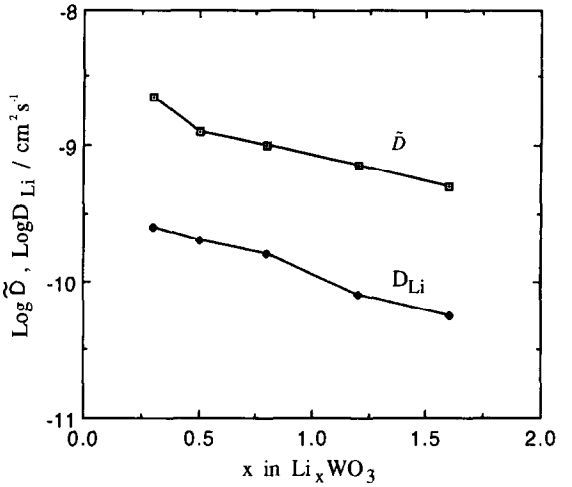

Fig. 8. Chemical and component diffusion coefficients of lithium as a function of x-values in Li_xWO_3.

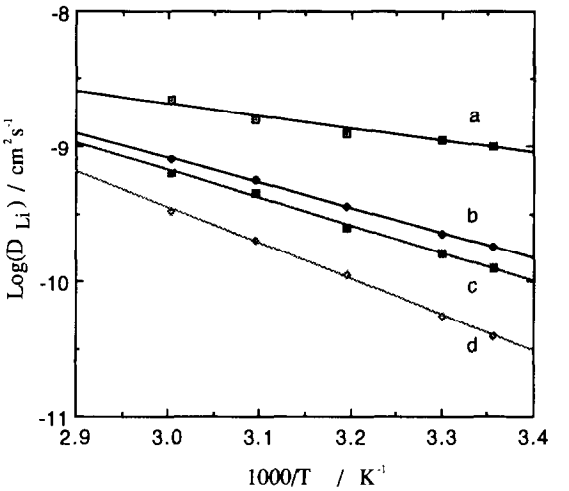

Fig. 9. Arrhenius plots of D_{Li} vs. $1000/T$ in Li_xWO_3 electrodes: (a) – $x = 0.1$; (b) – $x = 0.5$; (c) – $x = 0.8$; (d) – $x = 1.6$.

impedance responses were strongly dependent on the temperature variation. Deduced from the a.c. impedance data measured at different temperatures, the Arrhenius plots of component diffusion coefficient of lithium are given in Fig. 9 at different lithium compositions. Furthermore, the activation energies for lithium diffusion in the hexagonal tungsten trioxide obtained from the Arrhenius plots are given in Fig. 10, as a function of depth of lithium intercalation. The activation energies for the oxide are found to be ca. (25–73) kJ/mol in the ($x = 0.3$–1.6) range, being typical of diffusion in layered intercalation materials [14].

We had previously studied the kinetics of lithium intercalation into WO_3 with a monoclinic structure and several $nA_2O{\cdot}WO_3$ ($A = Na^+, K^+, NH_4^+$) having a hexagonal tungsten bronze structure by using an a.c. impedance method [3,14]. For the monoclinic WO_3 [3], the $\tilde{D}$ value obtained using 1 M $LiClO_4$–PC at 25°C was of the order of 10^{-11} cm^2/s and the activation enthalpy for lithium diffusion was ca. 60 kJ/mol. The $\tilde{D}$ value for the hexagonal WO_3 is one–two orders of magnitude higher and the activation energy for lithium diffusion is much lower, compared to the monoclinic WO_3. As seen in Fig. 1, the hexagonal

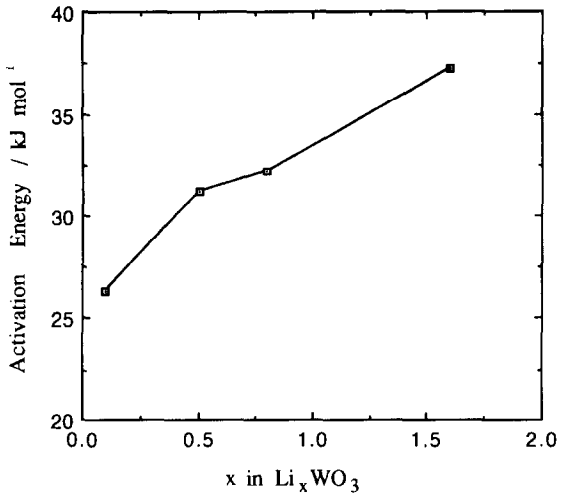

Fig. 10. Activation energies for lithium diffusion as a function of x-values in Li_xWO_3.

WO_3 contains large hexagonal tunnels surrounded by six WO_6 octahedra, through which two lithium atoms can be incorporated into the structure. The hexagonal WO_3 is found to have better kinetic behavior than that of the monoclinic WO_3, which reveals smaller tunnels surrounded by four WO_6 octahedra. On the other hand, in a series of $nA_2O{\cdot}WO_3$ ($A = Na^+, K^+, NH_4^+$) having a hexagonal tungsten bronze structure [14], the hexagonal tunnels may be occupied by the oxygen counter-ions of A cations in the A_2O component. Rietveld analysis of powder neutron diffraction data for $0.13\,Na_2O{\cdot}WO_3{\cdot}0.55H_2O$ [15] has shown that the oxygen counter-ions are located at the center of a large cavity in hexagonal tunnels together with water molecules, while the sodium ions are located in the window of the cavity. In several anhydrous forms $nA_2O{\cdot}WO_3$ ($A = Na^+, K^+, NH_4^+$), the maximum A_2O contents or the n-values are 0.14 [16], so that at least a half of the large cavities remain unoccupied. Therefore, lithium ions can be incorporated into the structure through the remaining empty hexagonal tunnels. The $\tilde{D}$ values in $Li_x[nA_2O{\cdot}WO_3](A = Na^+, K^+, NH_4^+)$ were of the order of 10^{-9} to 10^{-10} cm^2/s in the (0.5–1.5) range of x-values at 25°C and the activation energy for lithium diffusion in these oxides were in the (20–30) kJ/mol range. These kinetic parameters are close to those for hexagonal WO_3. Thus, the kinetic behavior of hexagonal WO_3 is quite similar to that of $nA_2O{\cdot}WO_3$ ($A = Na^+, K^+, NH_4^+$) having empty hexagonal tunnels. Furthermore, Joo et al. [17] have measured the $\tilde{D}$ values in $Li_x[0.165\ K_2O{\cdot}WO_3]$ thin film ($x = 0 - 0.3$) having a hexagonal tungsten bronze structure by using a galvanostatic transient method and have shown that the $\tilde{D}$ values are highly antisotropic, varying from 10^{-9} to 10^{-10} cm^2/s in the direction of the c-axis to ca. 10^{-7} cm^2/s in the direction of a-axis at room temperature. The $\tilde{D}$ value in hexagonal Li_xWO_3 ($x = 0.3 - 1.6$) are close to those along the c-axis in $Li_x[0.165\ K_2O{\cdot}WO_3]$. This suggests that the lithium intercalation into the polycrystalline hexagonal WO_3 electrode mainly takes place through the empty hexagonal tunnels.

References

[1] M.S. Whittingham, in B.V.B. Chowdari and S. Radhakrishna (Eds.), Solid State Devices, World Scientific, Singapore, 1988.
[2] K.P. Reis, A. Ramanan and M.S. Whittingham, J. Solid State Chem., 96 (1992) 31.
[3] Naoaki Kumagai. M. Abe, Nobuko Kumagai, J.P. Pereira-Ramos and K. Tanno, Solid State Ionics, 70/71 (1994) 451.
[4] J.P. Pereira-Ramos, R. Baddour-Haddour, N. Kumagai and K. Tanno, Electrochim. Act, 38 (1993) 431.
[5] K.P. Reis, A. Ramanan and M.S. Whittingham, Chem. Mater., 2 (1990) 219.
[6] B. Gerand, G. Nowogrocki, J. Guenot and M. Figlarz, J. Solid State Chem., 29 (1979) 429.
[7] Naoaki Kumagai, Nobuko Kumagai, Y. Umetsu and K, Tanno, Solid State Ionics, 86–88 (1996) 463.
[8] A.S. Nagelberg and W.L. Worrell, J. Solid State Chem., 29 (1979) 329.
[9] R. de Levie, Adv. Electrochem. Electrochem. Eng., 6 (1967) 329.
[10] J.E.B. Randles, Disc. Faraday Soc., 1 (1947) 11.
[11] C. Ho, I.D. Raistrick and R.A. Huggins, J. Electrochem. Soc., 127 (1980) 269.
[12] W. Weppner and R.A. Huggins, Ann. Rew. Mat. Sci., 8 (1978) 269.
[13] W. Dieterich, Solid State Ionic, 5 (1981) 21.
[14] Naoaki Kumagai, Y. Matsuura, Nobuko Kumagai and T. Tanno, J. Electrochem. Soc., 140 (1993) 3194.
[15] J. Guo, K.P. Reis and M.S. Whitingham, Solid State Ionics, 53 (1992) 305.
[16] N. Kumagai, Y. Matsuura, Y. Umestu and K. Tanno, Solid State Ionics, 53/56 (1992) 324.
[17] S. Joo, I.D. Raistrick and R.A. Huggins, Solid State Ionics, 17 (1985) 313.